Computer Simulations of Hyperbranched Polymers in Shear Flows

Alexey V. Lyulin,† David B. Adolf,* and Geoffrey R. Davies

IRC in Polymer Science and Technology, Department of Physics and Astronomy, University of Leeds, Leeds LS2 9JT, UK

Received October 31, 2000; Revised Manuscript Received February 21, 2001

ABSTRACT: Brownian dynamics simulations of hyperbranched polymers with different degrees of branching have been performed under the influence of simple shear flow. Hydrodynamic and excluded-volume interactions have been taken into account explicitly. Shear-thinning effects have been observed for all simulated degrees of branching. As the molecular weight of highly branched structures increases, the zero shear rate intrinsic viscosity reaches a maximum and begins to fall similar to the intrinsic viscosity behavior of perfectly branched dendrimers. In the absence of shear, static structure factors, $S(k)$, for hyperbranched polymers with the smallest number of monomers studied resemble those of a three-arm star. As the number of monomers increases and as the degree of branching increases, the $S(k)$ curves for the hyperbranched polymers begin to illustrate features associated with $S(k)$ curves for hard spheres. Further insight into the shape and interior density of these structures is obtained through the ratio of the radius of gyration, R_g, to the hydrodynamic radius, R_h. The ratio R_g/R_h is observed to approach unity as the number of monomers and the degree of branching increase.

1. Introduction

Macromolecular architecture has received considerable interest as the search for polymeric materials with new properties intensifies. Dendritic structures in particular have received much attention in recent years. These are treelike structures usually built from AB_2 monomers where each B group may react with one of the A group of another monomer. Fully branched, perfectly regular structures are referred to as dendrimers while imperfectly branched or irregular structures are referred to as hyperbranched polymers. One of the interesting properties of dendrimers is that a maximum[1] is observed in plots of intrinsic viscosity as a function of molecular weight in contrast to linear polymers which generally obey the Mark−Houwink equation

$$[\eta] = KM^a \tag{1}$$

where K and a are constants for a given polymer/solvent/temperature system.

Linear polymers thus exhibit a steady increase of intrinsic viscosity with increasing molecular weight while dendrimers offer the possibility of producing high molecular weight materials with low viscosity. They thus have potential applications in a number of areas such as viscosity modifiers or paints. The strategy for synthesizing dendrimers, however, includes several protection and deprotection steps making the synthesis time-consuming and expensive. A hyperbranched polymer (HP) is typically synthesized in a much more economical one-pot reaction, and the question therefore arises as to the extent to which these materials exhibit dendrimer-like properties.

In addition to their use as rheology modifiers, various other potential applications of HPs exist, such as thermoset resins,[2] toughening agents,[3] and nonlinear optical polymers.[4] Fundamental understanding of their behavior is therefore of general interest. Unravelling the structure−property relationships of hyperbranched materials is, however, doubly complex since the end result of a typical one-pot reaction is a highly disperse mixture of variable sized randomly branched molecules with very different topologies. This complicates experiments since the usefulness of characterization via conventional size exclusion chromatography is compromised due to the potentially similar hydrodynamic volumes of a highly branched dendrimer and a linear chain of fewer repeat units. Theoretical investigation is complicated, however, by the fact that systems are typically branched on a scale comparable with the Kuhn length, and hence equivalent random links and Gaussian chains do not exist. These experimental and theoretical complications make computer simulation, with its associated ability to control the simulated topology, a valuable way to obtain further insight and, in particular, to understand the geometry and rheology of hyperbranched materials.

Several experimental studies of hyperbranched studies have been reported, however, with varying degrees of characterization. In the early 1990s, Kim and Webster[5] reported the synthesis of hyperbranched polyphenylenes. Adding a small amount of this polymer to a polystyrene melt greatly reduced the melt viscosity. Later, Turner et al.[6,7] described the synthesis of all-aromatic hyperbranched polyesters with phenol and acetate end groups with a reported degree of branching of about 50%. Combination of size exclusion chromatography and differential viscometry indicated that the Mark−Houwink exponent for these polymers was considerably lower than that for the linear polystyrene standard. A maximum was not observed in the intrinsic viscosity as a function of molecular weight, however. More recently, Hobson and Feast[8] reported the synthesis of poly(amidoamine) hyperbranched systems which display a viscosity/molecular weight profile similar to that exhibited by dendrimers in that a trend of decreasing intrinsic viscosity with increasing molecular weight was observed (though the molecular weight was deduced and not directly measured). In general, there is general agreement that hyperbranched polymers exhibit reduced viscosities compared with equivalent linear poly-

† Present address: Eindhoven University of Technology, P.B.513, 5600 MB Eindhoven, The Netherlands.

* To whom correspondence should be addressed.

10.1021/ma0018796 CCC: $20.00
Published on Web 04/28/2001

mers, but the conditions for the existence of a maximum in the plot of intrinsic viscosity as a function of molecular weight are not clear.

One of the first simulations of HPs was performed by Widmann and Davies[9] using the simple bead−rod model together with an RIS Metropolis Monte Carlo procedure with intrinsic viscosities calculated from the radius of gyration. Aerts[10] simulated the intrinsic viscosity for the hyperbranched aliphatic polyesters described by Malmström et al.[11] and Hult et al.[12] using the bead model of Lescanec and Muthukumar.[13] Intrinsic viscosities were again calculated from the radius of gyration and also by using the hydrodynamic tensor approach. Both studies suggested that flexible HPs can exhibit a maximum in their intrinsic viscosity as a function of molecular weight. The maximum is, however, situated at a higher level of intrinsic viscosity and shifted to higher molecular weights than that for the equivalent dendrimer.

These simulations are open to criticism, however, in that Widmann and Davies used a phantom chain model, thus neglecting excluded-volume effects which are exacerbated in these highly crowded hyperbranched structures while Aerts employed a static building algorithm with no Monte Carlo or dynamic configurational relaxation. The deduction of the intrinsic viscosity from the radius of gyration of branched structures is also questionable.

This paper addresses these issues by employing Brownian dynamics (BD) techniques with a shear flow field to obtain the intrinsic viscosity (IV) data. This method allows the IV of a very dilute solution to be simulated over a broad range of shear rates. Hydrodynamic and excluded-volume interactions, which play an important role for dendrimers,[14] have been treated explicitly. The model and details of the simulation algorithms are presented in section 2. Our results are presented in section 3, and the main conclusions are summarized in section 4.

2. Details of the Model and Algorithms Used

A. Generation of Connectivity Tree and Characterization of Hyperbranched Molecules. Monomers within this paper are represented as beads where each bead consists of an A and two B groups. The number of monomer units, N, used within each simulated structure equaled 22, 46, 94, 190, or 382. Hyperbranched polymers are constructed from AB_2 monomers by creating the connectivity tree as described in ref 9. (The connectivity tree defines the bonding structure within a molecule.) Essentially, monomers are added one at a time to a growing molecule. At each addition, a B group from the growing molecule is randomly chosen and reacted with the A group of the monomer to be added. The starting monomer or "core" is a molecule with three B groups and no A group.

Different structures are generated by assigning different reaction probabilities to the unreacted B groups. Each unreacted B group whose neighbor on the same unit is also unreacted is given a reaction probability P_1. Alternatively, if the neighboring bead is already reacted, the unreacted bead is given a reaction probability P_2. The average topology of such hyperbranched molecules is controlled by the single parameter $k = P_2/P_1$. For values of $k < 1$, polymers with little branching are built and in the limit $k \rightarrow 0$ linear polymers result. For $k > 1$, highly branched polymers are built which, in the limit of $k \rightarrow \infty$, are fully branched structures but not perfect dendrimers since the terminal groups can belong to different generations. (i.e., they are at different distances from the core.)

For each value of N, several simulations are performed at different degrees of branching.The structures are classified according to N and their degrees of branching, DB. The degree of branching is defined[15] as

$$\mathrm{DB} = \frac{2D}{2D + L} \tag{2}$$

where D is the number of monomers with both B groups reacted (i.e., dendritic units) and L is the number of monomers with one reacted B group and one unreacted B group (i.e., linear units). The DB so defined varies from 0 for a linear chain to 1 for a perfect dendrimer or a fully branched hyperbranched polymer. This paper does not consider fully branched hyperbranched polymers so a DB value of 1 will correspond to the dendrimer with a focal core.

Previously, the DB was defined as the ratio of number of dendritic plus terminal monomers (i.e., both B groups unreacted) to the total number of monomers.[16] This definition, however, overestimates the DB of distributions of small molecules since unreacted monomers are typically counted as terminal units and contribute to the degree of branching. Also, the DB of linear polymers consisting of N monomers is equal to $1/N$ with the earlier definition and thus never zero. The definition of DB given by eq 2 avoids both of these problems.

For this work, DB values within the range of 0.2−0.8 are used. (For expediency, the data for perfect dendrimers, taken from a previous study,[14] are used for a DB of 1.)

The DB does not fully describe the connectivity, however, as is obvious from the fact that both perfect dendrimers and the less regular hyperbranched polymers can have a DB of 1. We therefore also use the Wiener index,[17] W, to characterize the different structures. This term was originated by Wiener during his investigations into the relationship between the atomistic connectivity of paraffin isomers and their boiling points. He defined this index as the cumulative distance between all pairs of carbon atoms within these molecules measured in terms of the number of intervening bonds between two atoms. This index also has been shown to correlate well with many physical and chemical molecular properties including molar volume, refractive index, heat of vaporization, and viscosity.[17]

In this work, the connectivity tree is used to determine the Wiener index. For a given number of monomers, W is always largest for the linear chain and smallest for a perfect dendritic structure. Its utility is demonstrated by the fact that, in the simulations of Widmann and Davies,[9] W exhibits a near perfect power-law correlation with the simulated intrinsic viscosities of molecules with the same molecular weight but different topologies.

B. Initial Configuration and Brownian Dynamics Algorithm. The Cartesian coordinates for the beads in the initial configuration of a given hyperbranched polymer are generated from its connectivity tree by a procedure due to Murat and Grest.[18] All bonded pairs of beads are separated by a fixed bond length, l. The distance between a newly added bead and all other beads is constrained to be larger than some distance $r_{\min} = 0.64l$. Bead overlaps are not allowed, and if a bead

cannot be inserted after a reasonable number of trials (e.g., 500−600), the whole structure is discarded and the procedure is started from the beginning with the same connectivity tree.

The Ermak−McCammon[19] algorithm is used for each integration step

$$\vec{r}_i = \vec{r}_i^0 + \Delta t/kT \sum_j \mathbf{D}_{ij}^0 \cdot \vec{F}_j^0 + \vec{v}_i^0 \cdot \Delta t + \vec{\Phi}_i^0(\Delta t) \qquad i = 0, ..., N \quad (3)$$

which has been used previously to simulate dumbbells and polymer chains under shear flow.[20] Here $\vec{r}_i^0$ is the position vector for bead i before a Brownian dynamics step, Δt, where the core is considered when $i = 0$, and kT is the Boltzmann factor. $\mathbf{D}_{ij}^0$ is the diffusion tensor, and $\vec{v}_i^0$ is the velocity of the solvent at the position of bead i where for steady shear flow $v_{i,x}^0 = y_i^0 \dot{\gamma}$. The solvent is represented as a structureless continuum with chain−solvent collisions mimicked by a random force $\vec{\Phi}_i^0$. The SHAKE algorithm[21] with a relative tolerance of 2×10^{-6} is used to maintain a fixed bond length. A Lennard-Jones [LJ] potential is invoked between all nonbonded beads i and j where the LJ σ parameter equals $0.80l$ and the LJ ϵ parameter equals $0.30kT$.[22] A cutoff distance of 2.5σ is also employed. No torsional or valence angle potentials are used. Hydrodynamic interactions (HI) are represented rigorously by means of the Rotne−Prager−Yamakawa interaction tensor.[23] The strength of the HI effects is set by the parameter $h^* = (3/\pi)^{1/2} a/l = (3/\pi)^{1/2} \zeta/(6\pi\eta_s l)$ where η_s represents the solvent viscosity and a is the Stokes hydrodynamic radius of a single bead. ζ denotes the friction coefficient of each bead. The data reported within this paper use $h^* = 0.25$ corresponding to the hydrodynamic radius $a = 0.257l$. This is the same value of h^* used within our simulations of dendrimers[14] whose intrinsic viscosity peaked at realistic generation values.

After generation of the initial configuration, the hyperbranched polymer is allowed to equilibrate for 100 000−500 000 Brownian dynamics time steps depending on its size and the magnitude of the shear rate. The attainment of steady state is monitored through the radius of gyration, R_g, and the components of the inertia tensor, **T**. Production runs typically consisted of 500 000−1 000 000 time steps, depending on the size of the system and magnitude of the shear rate. Other details of the simulation procedure are found within previous publications.[14,24]

C. Processing of Results. i. Structure Factor. The structure factor $S(\mathbf{k})$ is calculated along the three Cartesian axes in the absence of shear as

$$S(k_\alpha) = \left\langle \frac{1}{N^2} \left| \sum_{j=1}^{N} e^{ik_\alpha r_\alpha^j} \right|^2 \right\rangle \qquad \alpha = x, y, z \quad (4)$$

where the angular brackets denote averaging over all stored conformations for a particular trajectory. Averaging is made over the three projections, and finally the quantity $S(k) = (S(k_x) + S(k_y) + S(k_z))/3$ is reported as a function of the scattering vector which is varied over the range $0 < k < 2\pi/l$.

ii. Calculation of Viscosity. The dimensionless intrinsic viscosity $[\eta]^*$ is calculated according to

$$[\eta]^* = \frac{\eta - \eta_s}{nkT\lambda} \quad (5)$$

where the shear viscosity, η, is defined through the nondiagonal component of the shear stress tensor $\boldsymbol{\tau}$ as

$$\eta = -\frac{\tau_{xy}}{\dot{\gamma}} \quad (6)$$

The characteristic time λ in (5) is given by $\zeta l^2/12kT$, and n is the number density of molecules. In rheological experiments, the intrinsic viscosity is related not to a number density of polymer chains as used in eq 5 but rather to the concentration of chain monomers. For this reason, the normalized quantity $[\tilde{\eta}]_0 = [\eta]_0^*/N$ is also calculated where N is the total number of beads in the HP and the subscript 0 denotes a zero shear rate.

iii. Hydrodynamic Radius. The mean-square translational displacement of the center of mass (COM) of hyperbranched polymers has been calculated in the absence of shear flow. They are linear functions of time in all time regions covered by these simulations and are not shown. The COM diffusion coefficient for each HP is extracted from these data using the Einstein relationship $\langle \Delta r^2(t) \rangle = 6D_{com}t$. For nondraining polymers, the hydrodynamic radius, R_h, of the whole molecule is determined by the Stokes relation,

$$D_{com} = kT/6\pi\eta_s R_h \quad (7)$$

where η_s is the viscosity of the solvent. The hydrodynamic radius for an effective sphere representing the whole HP can also be calculated from its zero-shear intrinsic viscosity as[25]

$$[\tilde{\eta}]^* = \frac{10\pi}{3N} R_h^{3*} \quad (8)$$

The R_h values computed from these different approaches are very close to each other**,** the difference in all cases being less than 10%.

3. Results and Discussion

The following sections investigate the dependence of the simulated intrinsic viscosity, radius of gyration, and structure factors of HPs on their molecular weight, Wiener index, and the magnitude of the shear flow. The influence of the HI on the simulated properties is also reported. Dimensionless quantities are used and are represented by an asterisk where length (l), energy (kT), and translational friction $\zeta = 6\pi\eta_s a$ are set to unity. It follows that time is reduced by $\zeta l^2/kT$ and shear rate by $kT/\zeta l^2$. Dimensionless shear rates ranging from 0 to 10 are covered in this investigation. A dimensionless time step between $\Delta t^* = 1 \times 10^{-3}$ and 1×10^{-4} is used which decreases with increasing shear rate. The magnitude of the time step is chosen so that the maximum displacement of a bead is less than about 10% of the average bond length. Note that error bars for all plotted data points are smaller than the size of the symbols used within the figures unless otherwise indicated. Furthermore, lines are drawn between data points are aids to the eye unless otherwise indicated.

A. Intrinsic Viscosity. Figure 1a illustrates the shear thinning of the simulated intrinsic viscosity for HPs with different DB and different molecular weight N. At low shear rates, evidence of a Newtonian plateau in the intrinsic viscosity is observed with the onset of shear thinning occurring at smaller shear rates as the size of the HP increases. For the $N = 382$ DB $= 0.2$, 0.4, and 0.6 systems, an extra data point is included

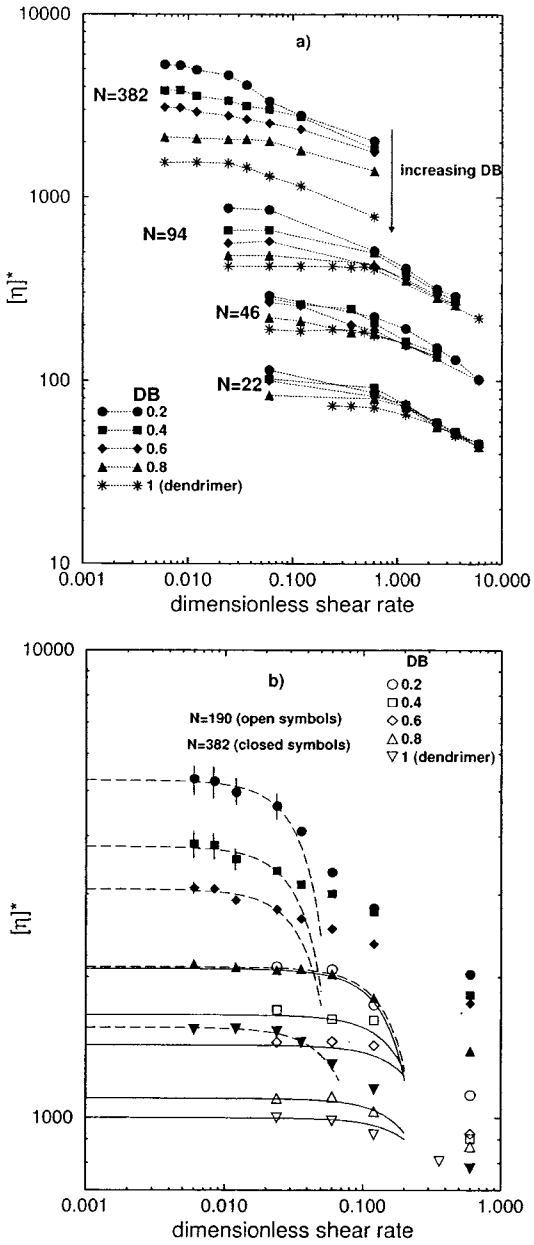

Figure 1. (a) Shear rate dependence of intrinsic viscosity for hyperbranched polymers of different molecular weight, N = 22, 46, 94, and 382, and different degrees of branching, from DB = 0.2 to DB = 1 (dendrimer). The N = 190 data are omitted for clarity. At a given value of N, the arrow indicates the direction of increasing degree of branching. Lines connecting symbols are drawn as an add to the eye. For the N = 382 DB = 0.2, 0.4, and 0.6 systems, an extra data point is included for a shear rate of 0.0084 to help better define the Newtonian plateau. (b) A more detailed perspective of the shear rate dependence of the intrinsic viscosity for the N = 190 (open symbols) and N = 382 (closed symbols) systems. The extrapolations using the lower shear rate data employed to extract zero shear viscosities are also shown as solid lines (N = 190) and dashed lines (N = 382).

for a shear rate of 0.0084 to help better define the Newtonian plateau. To appreciate the rates required to shear thin these structures, consider the dendrimer with N = 382 and DB = 1.0. Data in Figure 1a show that for this dendrimer the intrinsic viscosity begins to decrease at $\dot{\gamma}^*_{cr} \approx 0.02$. A typical solvent viscosity of 1 cP, a bond length l = 1.54 Å, and a temperature $T \sim 300$ K affords a characteristic time on the order of 10^{-11} s and a critical shear rate of 10^9 s^{-1}. Figure 1b illustrates the N = 190 (open symbols) and the N = 382 (closed symbols) data in greater detail, including error bars where they are larger than symbol size. Additionally, the extrapolations of the data used to extract the corresponding zero shear viscosities are also shown as solid lines (N = 190) and dashed lines (N = 382). The extrapolation process is discussed in greater detail below.

The conformation of an HP under the influence of shear flow is anisotropic. Snapshots of the HP with N = 382, DB = 0.2, and DB = 0.8 are shown in Figure 2 for the magnitude of shear rate $\dot{\gamma}^*$ = 0.6. For small degrees of branching, the HP is elongated in the direction of shear (i.e., the X axis) and is squeezed in the perpendicular direction (Figure 2a). At the same time the projection on the XZ plane reveals a much less compact and less elongated structure (Figure 2b). For the HP with DB = 0.8 at the same value of shear rate, the elongation in the shear direction is smaller (Figure 2c) with the XY projections being less elongated than the structure depicted in Figure 2a. The XZ projection of the HP with DB = 0.8 seen in Figure 2d is less sprawled out relative to the structure observed in Figure 2b. These snapshots suggest higher shear rates are needed to initiate shear thinning as the DB of the HPs increases.

As mentioned previously, zero shear rate viscosities $[\tilde{\eta}]_0$ are deduced by extrapolating the low shear rate data found in Figure 1a to zero shear rate. The resulting $[\tilde{\eta}]_0$ values are shown as a function of the molecular weight, N, in Figure 3 and as a function of the Wiener index, W, within Figure 4. The extrapolation is performed using 3−6 of the lowest shear rate data points for each hyperbranched polymer and the equation

$$[\tilde{\eta}]^* = a_0 - a_1\dot{\gamma}^{*2} \tag{9}$$

where a_0 and a_1 are fitting parameters. a_0 is related to the zero shear rate viscosity, and a_1 is related to the product of the zero shear rate viscosity and the square of a characteristic relaxation time for the hyperbranched polymer. This form is justified since the intrinsic viscosity does not depend on the direction of the shear and the intrinsic viscosity decreases with increasing shear rate (i.e., shear thinning). Many of the curves within Figure 1 exhibit a Newtonian plateau which supports the credibility of the extrapolated $[\tilde{\eta}]_0$ values. The presence of such a plateau is not as strongly observed for the N = 382 low DB systems which introduces more error into their extrapolated $[\tilde{\eta}]_0$ values.

The open symbols in Figure 3 indicate a steadily increasing molecular weight dependence of $[\tilde{\eta}]_0$ for linear chains with HI and excluded-volume interactions as reported by the authors in an earlier publication.[24] Starting with $N \sim 60$, the slope of this dependence is almost 0.5 as predicted by the theory.[26] For perfect dendrimers, the maximum in the dependence of $[\tilde{\eta}]_0$ vs molecular weight can be expected when the average volume of the polymer chain starts to increase slower than its molecular weight. Visualization of the instant conformations indeed reveals rather compact structures for HPs with DB ≥ 0.8 and N > 200, in contrast to the sparse conformations of HPs with smaller degrees of branching. Figure 3 indicates that all data for HPs lie between the two extreme cases for the linear chain and the perfect dendrimer. Even for DB = 0.2, the N dependence of $[\tilde{\eta}]_0$ for the HP is very different from that for the linear polymer. A maximum in the N dependence

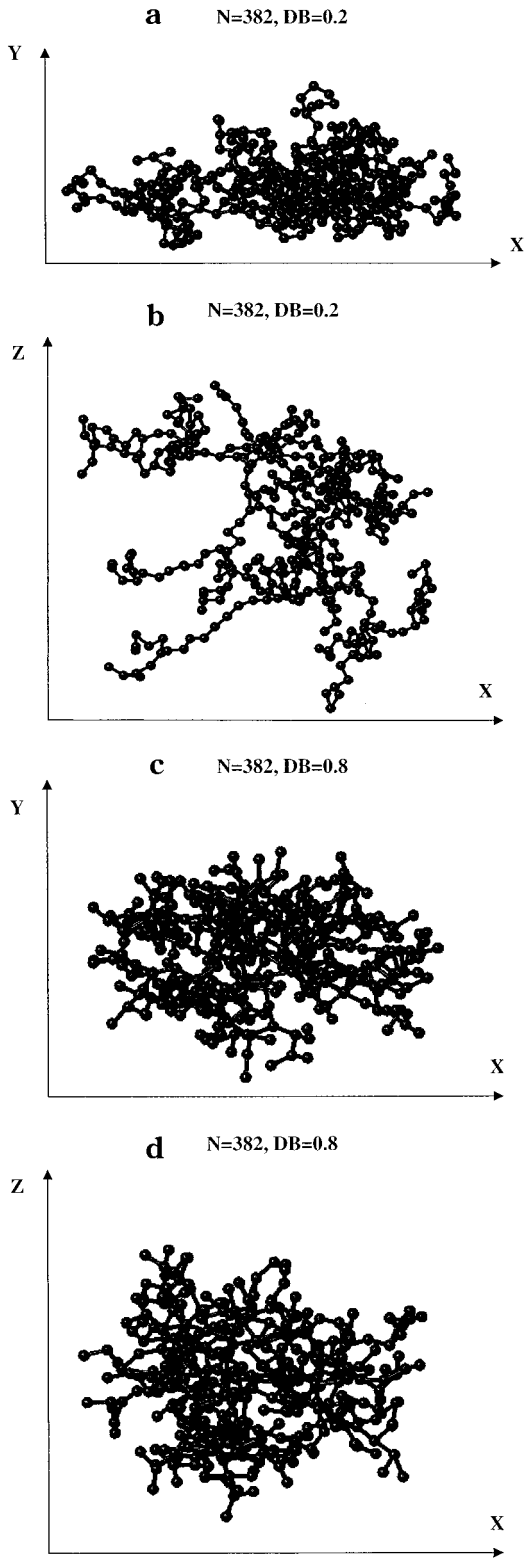

Figure 2. Snapshots of conformations of HP with $N = 382$ and different degrees of branching, DB = 0.2 (a, b) and DB = 0.8 (c, d) under the influence of shear flow. Projections on the XY (a, c) and XZ (b, d) planes are shown. Shear is directed along the X axis, and the magnitude of the shear rate is $\dot{\gamma}^* = 0.6$.

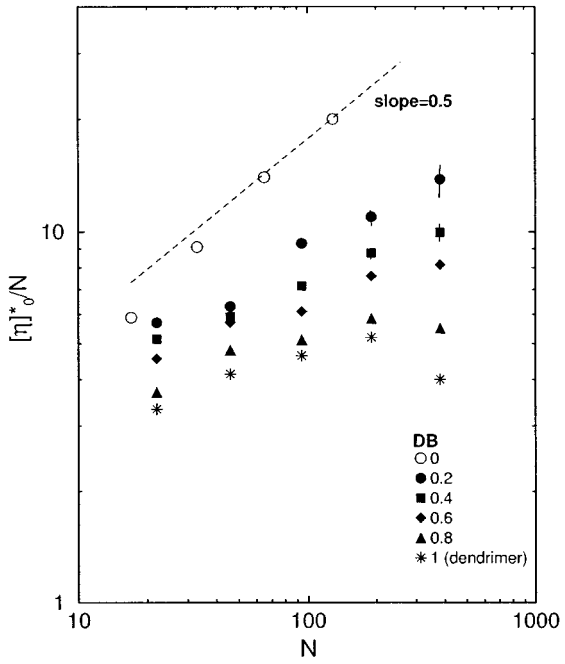

Figure 3. Molecular weight dependence of the zero shear rate intrinsic viscosity for HPs over a wide range of degrees of branching from linear chains (open circles, results from ref 24) to dendrimers (asterisks, results from ref 14). The dashed line of slope 0.5 represents the theoretical prediction for Gaussian chain in a Θ solvent.

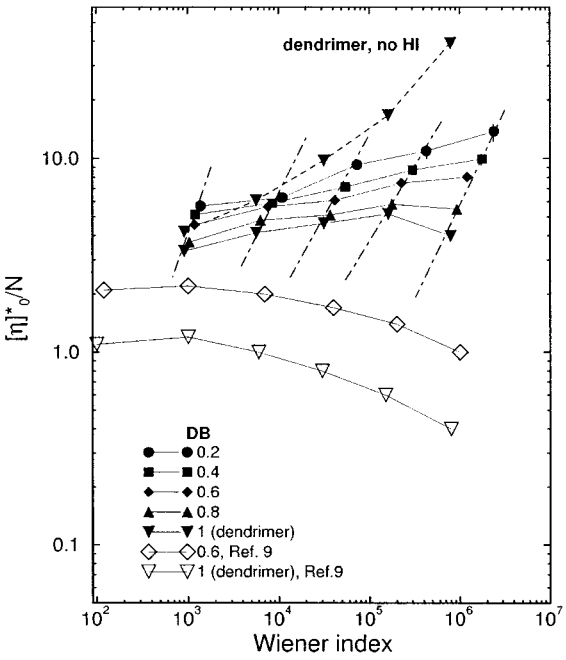

Figure 4. Zero shear rate intrinsic viscosity vs Wiener index of HPs at different degrees of branching. The dot−dashed line connects results with different DB values at a constant value of N (i.e., constant molecular weight). Simulation results for dendrimers without hydrodynamic interactions are shown by inverted triangles connected by a dashed line. Monte Carlo simulation results of ref 9 are shown by open symbols.

of $[\tilde{\eta}]_0$ for the HP with DB = 0.8 is observed in Figure 3, which is not as intense as that observed for the data associated with the dendrimer (i.e., DB = 1.0). Data for the HP with DB = 0.6 are beginning to level off in the area where the maxima in the DB = 0.8 and DB = 1.0 data occur, suggesting the possible existence of a peak at higher values of N. Similar conclusions are not made for the lower DB data in light of the larger than typical error for the $N = 382$ system.

The relationship between $[\tilde{\eta}]_0$ and the Wiener index, W, of the same HPs is shown in Figure 4. Simulated results for dendrimers but without hydrodynamic interactions are also shown by a dashed line connecting

inverted filled triangles. Results for the freely draining HPs indicate a strong increase in intrinsic viscosity with increasing Wiener index. Inclusion of HI changes the results dramatically, leading to the pronounced maxima at DB = 0.8 and 1.0. At constant molecular weight denoted by the dot−dashed lines, $[\tilde{\eta}]_0 \sim W^a$ where a = 1.6, 1.4, 1.2, 1.1, and 1.1 when looking left to right at the five sets of data with each set comprised of five different filled symbols connected by dashed lines. This affords an average slope of ∼1.3, which is less than the value of 1.5−1.6 indicated within the work of Widmann and Davies. [9] To enable further comparisons, results for HPs from the Widmann and Davies work with DB = 0.6 and DB = 1 are included within Figure 4 as unfilled symbols. These HPs also exhibit maxima on their W dependence of intrinsic viscosity but lie significantly below the analogous plots from this study. This behavior can be attributed to the use of excluded volume within the current study but not within that of Widmann and Davies. Furthermore, the peak in the simulated intrinsic viscosity is shifted to higher generations relative to the data of Widmann and Davies. The observed intrinsic viscosity peaks within the current work occur around the fourth or fifth generation. This is the vicinity of an estimated peak in the intrinsic viscosity of a dendrimer based on its hydrodynamic volume increasing as the third power of the generation number (g^3) and the molecular weight increasing as 2^g. With intrinsic viscosity ∼ hydrodynamic volume/mass ∼ $g^3/2^g$, a maximum is found at g_{max} = 3/ln 2 ∼ 4.3.

B. Structure Factor in the Absence of Shear. Single molecule structure factors are displayed in Kratky format in Figure 5a−c for HPs of different molecular weights and degrees of branching. Curves for molecules other than HPs and dendrimers are plotted within these figures for comparative purposes. Curves are included in each figure for a Gaussian coil with a radius of gyration equal to the figure's HP with DB = 0.2. Similarly, curves are included in each figure for a hard sphere with a radius of gyration equal to the figure's dendrimer. The curves for the three-arm star polymers with the same radius of gyration as for HPs with DB = 0.2 have been calculated in separate Brownian dynamics simulations using the HB excluded-volume interaction parameters and without hydrodynamic interactions. The simulated HPs have structure factors very different from that of an ideal Gaussian coil and the three-arm stars except for the N = 22 HP whose DB = 0.2 curve is very similar to that of the three-arm star. Furthermore, Figure 5c reveals the secondary Kratky peak in the region of $4 < kR_g < 6$ begins to appear in the N = 94 dendrimer.

C. Hydrodynamic Radius. Further information regarding the shape of the simulated HPs is obtained through the ratio of the hydrodynamic radius, R_h, to the radius of gyration, R_g. The ratio R_g/R_h varies from 0.73 to 0.80 for linear unperturbed polymers to ∼1.0 for regular star polymers to 1.29 for hard spheres of uniform density.[27] This ratio is plotted in Figure 6 as a function of the degree of branching of the HP in the absence of shear flow where the hydrodynamic radius is calculated as an average of eqs 7 and 8. The lines join data with the same value of N and serve as an aid to the eye. The figure reveals that the ratio tends to 1 with increase N and increasing DB. This is in good agreement with the findings of Ishizu et al.[27] on

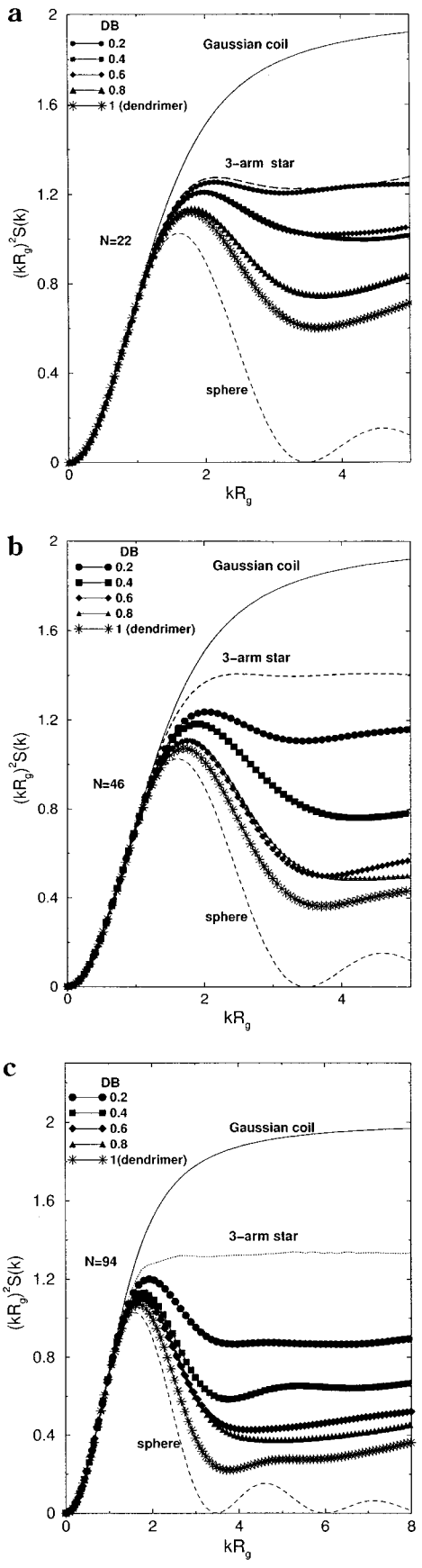

Figure 5. Kratky plots of the static structure factors for HPs of different molecular weight, N = 22 (a), N = 46 (b), and N = 94 (c) for different degrees of branching. Analytical results for corresponding Gaussian coils and hard spheres and simulation results for 3-arms star polymers with excluded-volume interactions are also shown.

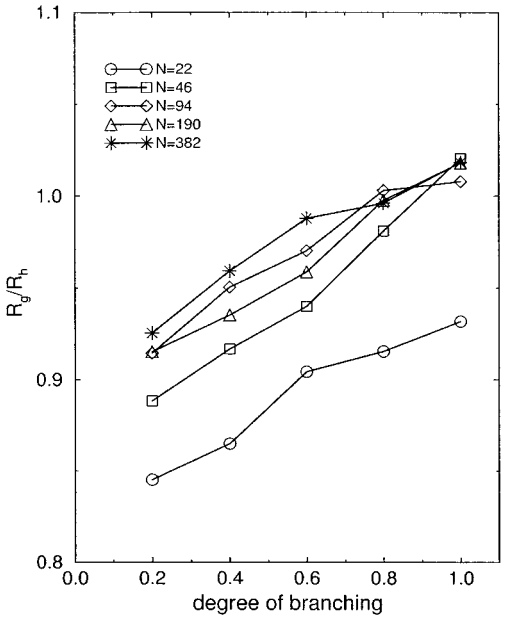

Figure 6. Dependence of the ratio R_g/R_h on the degree of branching at various values of N. Lines connecting symbols are drawn as a guide to the eye.

hyperbranched polymers derived from copolymerization of poly(4-methylstyrene)-*block*-polystyrene.

4. Conclusions

Computer simulations of hyperbranched polymers with different degrees of branching under shear with excluded-volume and hydrodynamic interactions have been performed. HPs with smaller amounts of branching (i.e., low values of DB) reveal sparse structures while those with larger amounts of branching (i.e., high values of DB) possess very compact structures. Under shear, the structures become anisotropic being elongated in the direction of shear and squeezed perpendicular to it. For a fixed number of monomers units N, simulated HP viscosities are larger than the analogous quantity for the dendrimer, and all HPs exhibit shear thinning similar to that of perfect dendrimers.[14] However, the magnitude of the critical shear rate at the onset of shear thinning shifts to smaller values as compared to dendrimers. The zero-shear intrinsic viscosity of HPs does peak at a critical molecular weight, but the peak is less pronounced relative to that observed for dendrimers. Comparisons with other simulation efforts reveal that as the molecular weight is varied at a fixed DB, the explicit inclusion of hydrodynamic and excluded-volume interactions affords high values of simulated viscosities and shifts any maximum in the simulated intrinsic viscosity to higher molecular weight. As DB and N are increased, static structure factors reveal how the HP shape begins to approach a constant density sphere, and plots of R_g/R_h vs the degree of branching are in good agreement with experimental findings.

Acknowledgment. The authors acknowledge the EPSRC for financial support of this study (GR/L79229) and a 1997 Joint Research Equipment Initiative for computer time.

References and Notes

(1) (a)Mourey, T. H.; Turner, S. R.; Rubinstein, M.; Frechet, J. M. J.; Hawker, C. J.; Wooley, K. L. *Macromolecules* **1992**, *25*, 2401. (b) Hawker, C. J.; Farrington, P. J.; Mackay, M. E.; Wooley, K. L.; Frechet, J. M. J. *J. Am. Chem. Soc.* **1995**, *117*, 4409.
(2) Johansson, M.; Malmström, E.; Hult, A. *J. Polym. Sci., Part A: Polym. Chem.* **1993**, *31*, 619.
(3) Boogh, L.; Pettersson, B.; Japon, S.; Månson, J.-A. E. *Proc. ICCM-10, Whistler, British Columbia, Canada* **1995**, *6*, 389.
(4) Zhang, Y.; Wada, T.; Sasabe, H. *Polymer* **1997**, *38*, 2893.
(5) Kim, Y. H.; Webster, O. W. *J. Am. Chem. Soc.* **1990**, *112*, 4592.
(6) Turner, S. R.; Voit, B. I.; Mourey, T. H. *Macromolecules* **1993**, *26*, 4617.
(7) Turner, S. R.; Walter, F.; Voit, B. I.; Mourey, T. H. *Macromolecules* **1994**, *27*, 1611.
(8) Hobson, L. J.; Feast, W. J. *Polymer* **1999**, *40*, 1279.
(9) Widmann, A. H.; Davies, G. R. *Comput. Theor. Polym. Sci.* **1998**, *8*, 191.
(10) Aerts, J. *Comput. Theor. Polym. Sci.* **1998**, *2*, 49.
(11) Malmström, E.; Johansson, M.; Hult, A. *Macromolecules* **1995**, *28*, 1698.
(12) Hult, A.; Johansson, M.; Malmström, E. *Macromol. Symp.* **1995**, *98*, 1159.
(13) Lescanec, R. L.; Muthukumar, M. *Macromolecules* **1990**, *23*, 2280.
(14) Lyulin, A.; Davies, G. R.; Adolf, D. B. *Macromolecules* **2000**, *33*, 3294.
(15) Hölter, D.; Burgath, A.; Frey, H. *Acta Polym.* **1997**, *48*, 30.
(16) Hawker, C. J.; Lee, R.; Fréchet, J. M. J. *J. Am. Chem. Soc.* **1992**, *113*, 4583.
(17) (a) Wiener, H. *J. Am. Chem. Soc.* **1947**, *69*, 17. (b) Gutman, I.; Yeh, Y.-N.; Lee, S.-L.; Luo, Y.-L. *Ind. J. Chem.* **1993**, *32A*, 651.
(18) Murat, M.; Grest, G. *Macromolecules* **1996**, *29*, 1278.
(19) Ermak, D. L.; McCammon, J. A. *J. Chem. Phys.* **1978**, *69*, 1352.
(20) Rudisill, J. W.; Fetsko, S. W.; Cummings, P. T. *Comput. Polym. Sci.* **1993**, *3*, 23. Diaz, F. G.; Garcia de la Torre, J.; Freire, J. *Polymer* **1989**, *30*, 259.
(21) Ryckaert, J.-P.; Bellemans, A. *Chem. Phys. Lett.* **1975**, *30*, 123.
(22) Freire, J. J.; Rey, A.; García de la Torre, J. *Macromolecules* **1986**, *19*, 457.
(23) Rotne, J.; Prager, S. *J. Chem. Phys.* **1969**, *50*, 4831.
(24) Lyulin, A. V.; Adolf, D. B.; Davies, G. R. *J. Chem. Phys.* **1999**, *111*, 758.
(25) Doi, M.; Edwards, S. F. *The Theory of Polymer Dynamics*; Oxford University Press: New York, 1986.
(26) Flory, P. J. *Principles of Polymer Chemistry*; Cornell University Press: Ithaca, NY, 1953; Chapter 5.
(27) Ishizu, K.; Takahashi, D.; Takeda, H. *Polymer* **2000**, *41*, 6081.

MA0018796